NASA CR-168186
REPORT NO. GDC-SP-83-041
CONTRACT NO. NAS3-22252

ANALYSIS OF THE REFLECTIVE MULTIBANDGAP SOLAR CELL CONCEPT

July 1983

GENERAL DYNAMICS
Convair Division

1. Report No.	2. Government Accession No.	3. Recipient's Catalog No.
NASA CR-168186		

4. Title and Subtitle	5. Report Date
ANALYSIS OF THE REFLECTIVE MULTIBANDGAP SOLAR CELL CONCEPT	July 1983
	6. Performing Organization Code
7. Author(s)	8. Performing Organization Report No.
T.G. Stern	GDC-SP-83-041
	10. Work Unit No.
9. Performing Organization Name and Address	11. Contract or Grant No.
General Dynamics Convair Division San Diego, California	NAS3-22252
	13. Type of Report and Period Covered
12. Sponsoring Agency Name and Address	Contractor Report
National Aeronautics and Space Administration Washington, D.C. 20546	14. Sponsoring Agency Code

15. Supplementary Notes

Project Manager, Bernard L. Sater, Advanced Energetics Program, NASA Lewis Research Center, Cleveland Ohio

16. Abstract

A new and unique approach to improving photovoltaic conversion efficiency, the reflective multibandgap solar cell concept, was examined. This concept uses back surface reflectors and light trapping with several physically separated cells of different bandgaps to make more effective use of energy from different portions of the solar spectrum. Preliminary tests performed under General Dynamics Independent Research and Development (IRAD) funding have demonstrated the capability for achieving in excess of 20% conversion efficiency with aluminum gallium arsenide and silicon. This study analyzed the ultimate potential for high conversion efficiency with 2, 3, 4, and 5 different bandgap materials, determined the appropriate bandgaps needed to achieve this optimized efficiency, and identified potential problems or constraints. The analysis indicated that an improvement in efficiency of better than 40% could be attained in this multibandgap approach, compared to a single-bandgap converter under the same assumptions. Increased absorption loss on the back surface reflector was found to incur a minimal penalty on efficiency for two- and three-bandgap systems. Current models for bulk absorption losses in III-V materials were found to be inadequate for explaining laboratory observed transmission losses. Recommendations included the continued development of high bandgap back surface reflector cells and basic research on semiconductor absorption mechanisms.

17. Key Words (Suggested by Author(s))	18. Distribution Statement
Photovoltaics Multibandgap Spectrum-splitting Back surface reflectors	Unclassified - unlimited

19. Security Classif. (of this report)	20. Security Classif. (of this page)	21. No. of Pages	22. Price*
Unclassified	Unclassified	41	

* For sale by the National Technical Information Service, Springfield, Virginia 22161

FOREWORD

This final report was prepared by General Dynamics Convair Division for NASA Lewis Research Center in compliance with Contract NAS3-22252.

The principal results were developed during the period of performance October 15, 1982 to April 15, 1983. A final presentation of the study results was conducted on May 11, 1983.

The study was conducted in Convair's Advanced Space Programs Department, directed by W. F. Rector III. The NASA project manager is B. L. Sater of the LeRC Advanced Energetics Program. The study manager is T. G. Stern of Convair's Advanced Energy Systems Department.

For further information contact:

B. L. Sater
NAS/LeRC
Cleveland, Ohio 44135
(216) 433-4000 x5333

T. G. Stern
General Dynamics Convair Division
San Diego, California 92138
(619) 277-8900 x2204

TABLE OF CONTENTS

LIST OF FIGURES

LIST OF TABLES

ACRONYMS AND ABBREVIATIONS

AlGaAs	aluminum gallium arsenide
AM 1	air mass 1, sunlight passing through 1 atmosphere, i.e., terrestrial insolation
AM 0	air mass 0, extraterrestrial insolation
AR	anti-reflection
BSR	back surface reflector
C, CR	concentration ratio
E_g	bandgap
eV	electron volt
FF	fill factor
GaAs	gallium arsenide
I_{sc}	short-circuit current
IRAD	independent research and development
J_s	solar cell short circuit
J_o	solar cell diode current
N	dopant concentration
n_i	index of refraction
Q_i	quantum efficiency
q	quantum charge (of an electron)
Si	silicon
UV	ultraviolet
V_{oc}	open-circuit voltage
VF	voltage factor
$\alpha(\lambda)$	absorption coefficient as a function of wavelength
λ	wavelength
η	efficiency in converting incident sunlight into electricity
μm	micrometer
nm	nanometer

SUMMARY

To meet the higher power needs of future spacecraft, more efficient solar arrays are needed. Increasing conversion efficiency would improve specific power per unit weight and volume and reduce required array size. This would improve the structural dynamics and survivability, and reduce array costs ($/watt). Current multibandgap approaches involve the use of dichroic mirrors or monolithic multilayer structures that require current and lattice matching. The objective of this program was to examine and analyze a new and unique approach to improving efficiency, the reflective multibandgap solar cell concept. This concept, which uses back surface reflectors and light trapping with several physically separated cells of different bandgaps, avoids the problems associated with other multibandgap approaches. Preliminary tests performed under General Dynamics Independent Research and Development (IRAD) funding have demonstrated the capability for achieving in excess of 20% conversion efficiency with aluminum gallium arsenide and silicon. This study analyzed the ultimate potential for high conversion efficiency with 2, 3, 4, and 5 different bandgap materials, determined the appropriate bandgaps needed to achieve this optimized efficiency, and identified potential problems or constraints. The approach to this analysis included the development of a computer simulation program that divides the solar spectrum into component wavelength bands, traces the power flows throughout the system, determines useful energy absorbed by the solar cells, estimates losses due to competing processes and thermal loads on the system, and calculates the solar cells' responses.

The analysis indicated that an improvement in efficiency of better than 40% could be attained in this multibandgap approach, compared to a single-bandgap converter under the same assumptions. Increased absorption loss on the back surface reflector was found to incur a minimal penalty on efficiency for two- and three-bandgap systems. Current models for bulk absorption losses in III-V materials were found to be inadequate for explaining laboratory observed transmission losses. Recommendations included the continued development of high bandgap back surface reflector cells and basic research on semiconductor absorption mechanisms.

SECTION 1
INTRODUCTION

1.1 THE NEED FOR HIGHER EFFICIENCY SOLAR ARRAYS

Spacecraft being designed for launch by the Space Transportation System (STS) over the next several years will require higher power levels – tens of kilowatts – and increased life and durability in the face of natural and hostile environments. The increased size of today's low efficiency planar arrays poses many problems as they grow to meet these needs. Large solar wings have undesirable structural qualities, including low loading capability, very low natural frequency, and underdamping. At these high power levels, weight and volume restrictions in the Shuttle payload bay become critical. Finally, the larger a solar wing grows, the more difficult it becomes to stiffen, shield, and harden in a cost- and weight-effective manner. If the photovoltaic conversion efficiency can be increased from its current 10-15%, many of these concerns could be greatly alleviated. It has been shown, both analytically and with laboratory demonstration data, that the use of multibandgap (sometimes called multicolor) solar cell arrays can roughly double this conversion efficiency to 20-30%. The approach of using multibandgap photovoltaics involves the conversion of the high-energy (blue) spectral band of sunlight by high-bandgap (i.e., higher voltage) solar cells, the medium energy (yellow) band by a medium-bandgap solar cell, and the low-energy (red) band by a low-bandgap solar cell and so on. The more bandgaps used, the greater the potential for efficiency improvements.

1.2 CURRENT APPROACHES TO MULTIBANDGAP SOLAR ARRAYS

Two approaches considered for implementing multibandgaps are the use of dichroic mirrors and the fabrication of monolithic multibandgap cells. In the first approach, a multilayer dichroic mirror (Figure 1-1) reflects a spectral band to one solar cell of appropriate bandgap while transmitting the remaining sunlight to a second dichroic mirror.[1,2] The second mirror in turn reflects a portion of the remaining light to a second solar cell of different bandgap, and transmits the remaining light to a third solar cell of different bandgap.

The second approach (Figure 1-2) requires the growth of the various bandgap materials onto a single substrate.[3] The highest bandgap material on the top of the stack absorbs and converts the high energy photons while transmitting the remaining light to the next layer, and so on. The main issues associated with these structures are 1) mitigating the differences in lattice constant and thermal expansion coefficients of the different materials, 2) matching the currents from each layer to prevent current-limiting recombination losses, and 3) providing good electrical contact between layers, usually by incorporating tunnel junctions.

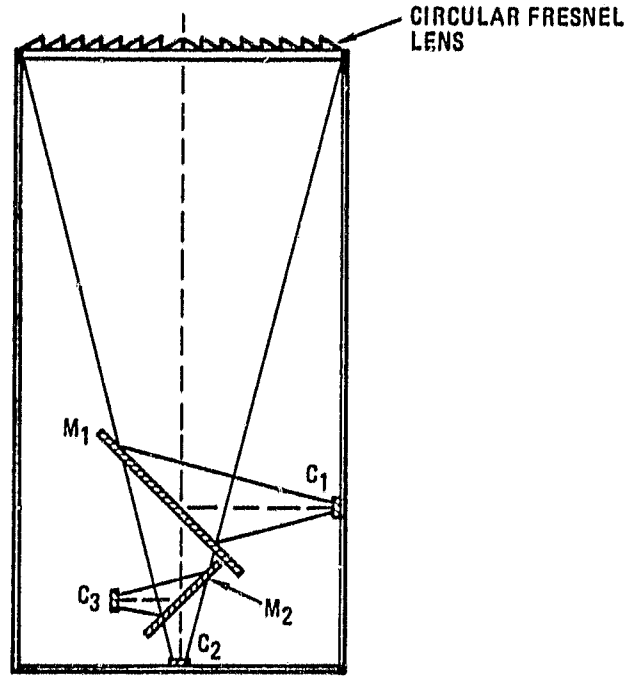

266.955-3

Figure 1-1. Multibandgap Approach Using Dichroic Mirrors

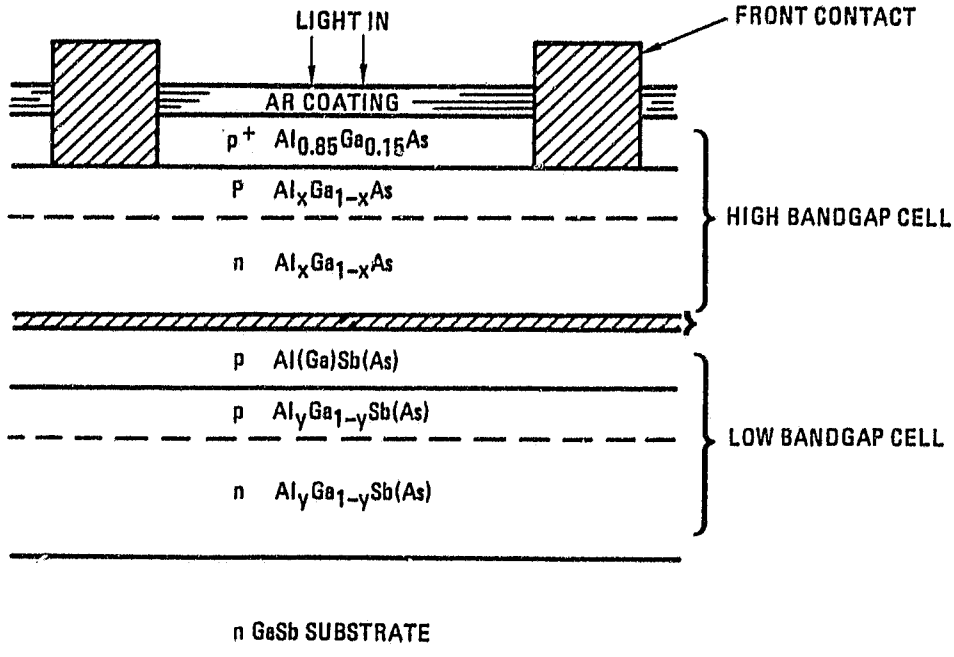

266.955-4

Figure 1-2. Multilayer Monolithic Multibandgap Solar Cell

The multibandgap approach investigated in this effort does not require multilayer dichroic mirrors, lattice matching, current matching, a complex multilayer structure, or tunnel junctions, and it can be achieved with current technology.

1.3 REFLECTIVE MULTIBANDGAP SOLAR CELL CONCEPT

The dual-bandgap solar cell assembly shown in Figure 1-3 was conceived and developed under General Dynamics IRAD.[4] This spectrum splitting concept takes advantage of two properties of the aluminum gallium arsenide (AlGaAs) high-bandgap solar cell; namely, 1) its sharp absorption edge, i.e., its transparency to photons with less than its bandgap energy, and 2) its back surface reflector that has a high reflectance to these lower energy photons.

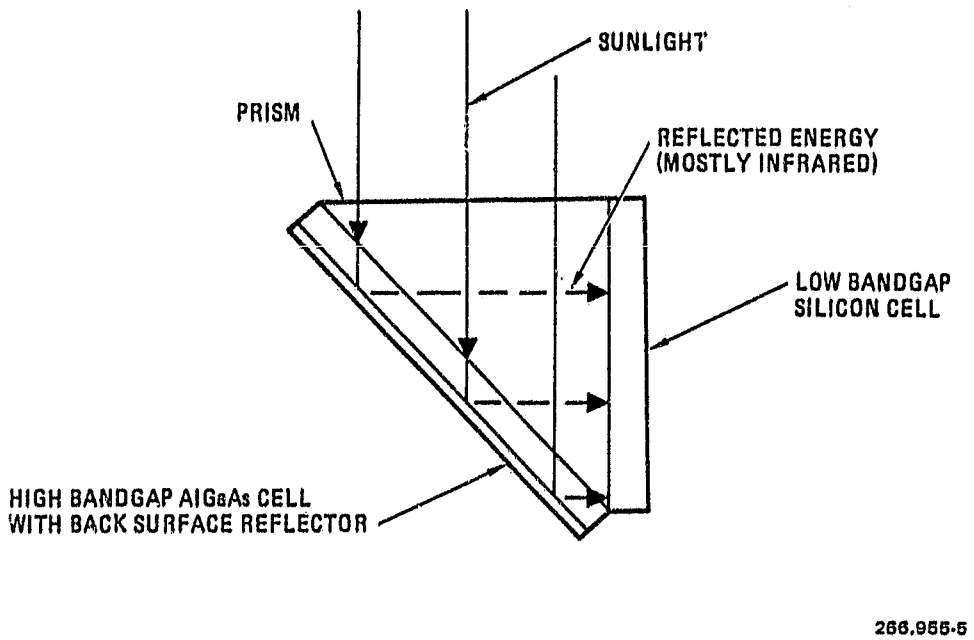

Figure 1-3. A Dual-bandgap Reflective Design Developed on IRAD

The sunlight entering the prism of Figure 1-3 is parallel with respect to the silicon cell, but is assumed to have dispersion in and out of the plane of the paper as it arrives from a one-axis trough concentrator that is appropriately oriented. The prism is incorporated in the assembly to prevent light from escaping out its triangular faces as a result of this dispersion. Light trapping resulting from total internal reflection within the glass is highly efficient since total internal reflectivity is greater than 99%. Additionally the incidence angles of the flux entering the prism entrance aperture are reduced as they enter the denser glass medium.

Light entering the prism is passed on to the AlGaAs cell, which absorbs and converts to electricity those photons with energy higher than its bandgap. In this case, the spectral band of sunlight with wavelength $\lambda < 750$ nm is absorbed by the AlGaAs cell. The remaining sunlight is transmitted through the AlGaAs cell, reflected off its back surface reflector, and is thereby directed to the lowerbandgap silicon cell that can efficiently convert the spectral band with wavelengths $750 < \lambda < 1100$ nm. This prototype dual-bandgap receiver was built with pieceparts shown in Figure 1-4 as part of the IRAD work. The best prototype units achieved over 20% conversion efficiency at AM 1 (terrestrial insolation).

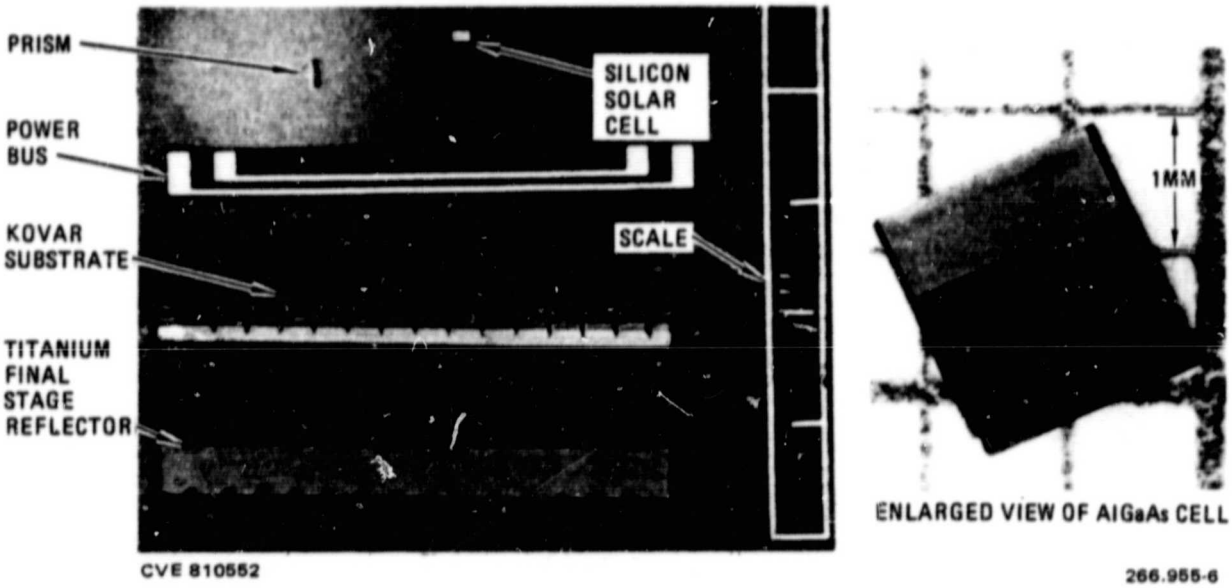

Figure 1-4. Pieceparts for the IRAD Dual-bandgap Design

The reflective multibandgap approach can be extended to any number of bandgaps consistent with weight and cost trade-offs. Figure 1-5 shows four bandgaps. For a five-cell system, the fifth cell would occupy the exit aperture. The glass parallelepiped again prevents rays from escaping out the sides of the assembly by total internal reflection. Each of the cells in this assembly requires a sharp absorption edge that can be accomplished with solar cells of the quaternary system AlGaAsSb. By varying the relative quantities of aluminum, gallium, arsenic, and antimony, any bandgap solar cell material from 0.7 to 2.2 eV can be provided having high quantum efficiency and sharp absorption edge.

Two additional advantages of this approach should be noted. First, unused energy (i.e., photons with energy less than the lowest bandgap in the system) can exit the assembly unabsorbed. This reduces the thermal load and, thus,

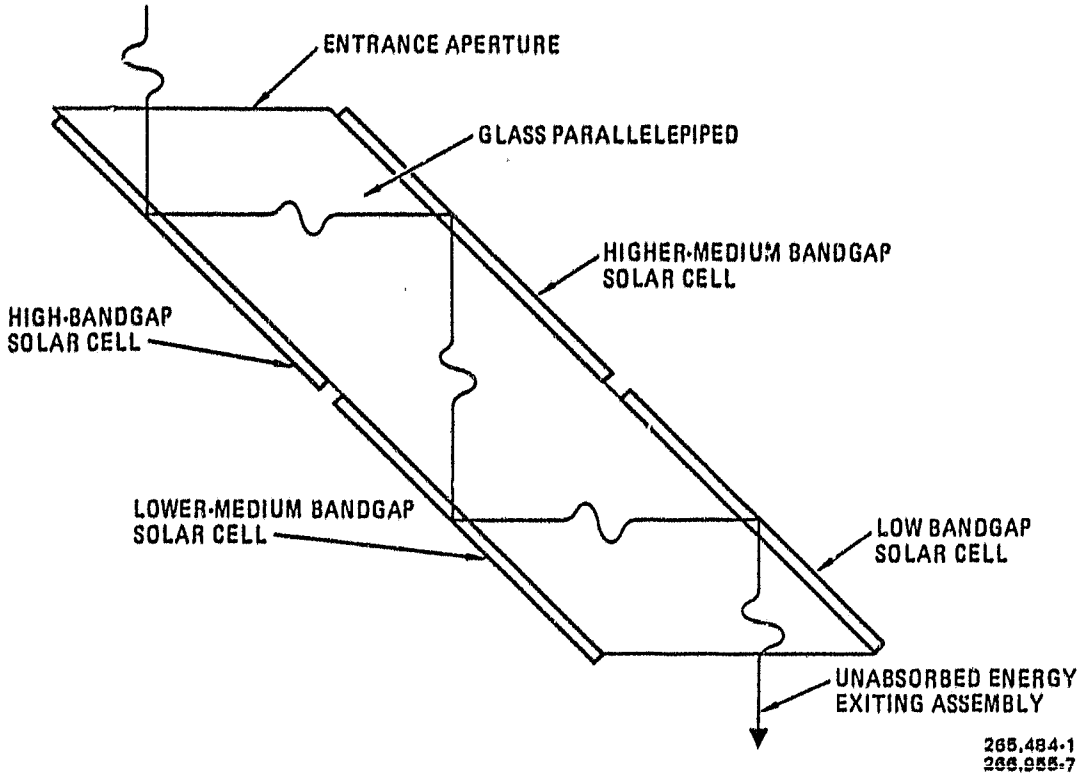

Figure 1-5. Extension of the Dual-bandgap to Multibandgap Design

the temperature of the assembly, and increases the efficiency of each solar cell. Secondly, grid and surface reflection (that can reduce converted energy by 10% or more in conventional solar cells) is greatly reduced. Grid and surface reflection from the high-bandgap cell passes this energy to the medium-bandgap solar cell where it can still be converted, although not as efficiently. Only the lowest bandgap cell will suffer total grid loss, but since it will receive only a small portion of the total incident flux, the total grid reflection loss of the system will be minimal.

One possible constraint on the system that requires consideration is the effect of free-carrier absorption. This effect occurs in the n-type bulk upon which the active photovoltaic junction layer is grown. Since this absorption increases as the cube of wavelength it could potentially limit the spread between the highest and the lowest bandgaps used in the system. One way to reduce this effect, which has been explored in the IRAD dual-bandgap development, is to use a thinned cell structure. The AlGaAs cells grown by chemical vapor deposition for the General Dynamics IRAD program have achieved thicknesses as low as 5 microns (0.2 mils). At these thicknesses, free-carrier absorption becomes negligible throughout the wavelength range of interest.

1.3.1 CELL POWER OUTPUTS. Each solar cell in the multibandgap system will absorb a spectrum of useful light (i.e., photons with energy greater than the cell bandgap that can generate electron-hole pairs), as well as a spectrum of unproductive light (because of absorption by the back surface reflector, by the grid, and by free carriers in the bulk). The usefully absorbed photons are converted with some quantum efficiency to electron-hole pairs, which are collected at the solar cell's open circuit potential V_{OC}. Since the absorbed photons have an energy that is, in general, greater than the quantum power out of the cell, a thermal load called "blue-loss" is generated during the photovoltaic process. Figure 1-6 is a graphic representation of this absorption and conversion process for a three-bandgap system, showing the nonproductive absorption losses at each cell, the useful absorbed spectrum, and the electrical power output as areas under the spectral distribution curve of solar irradiance.

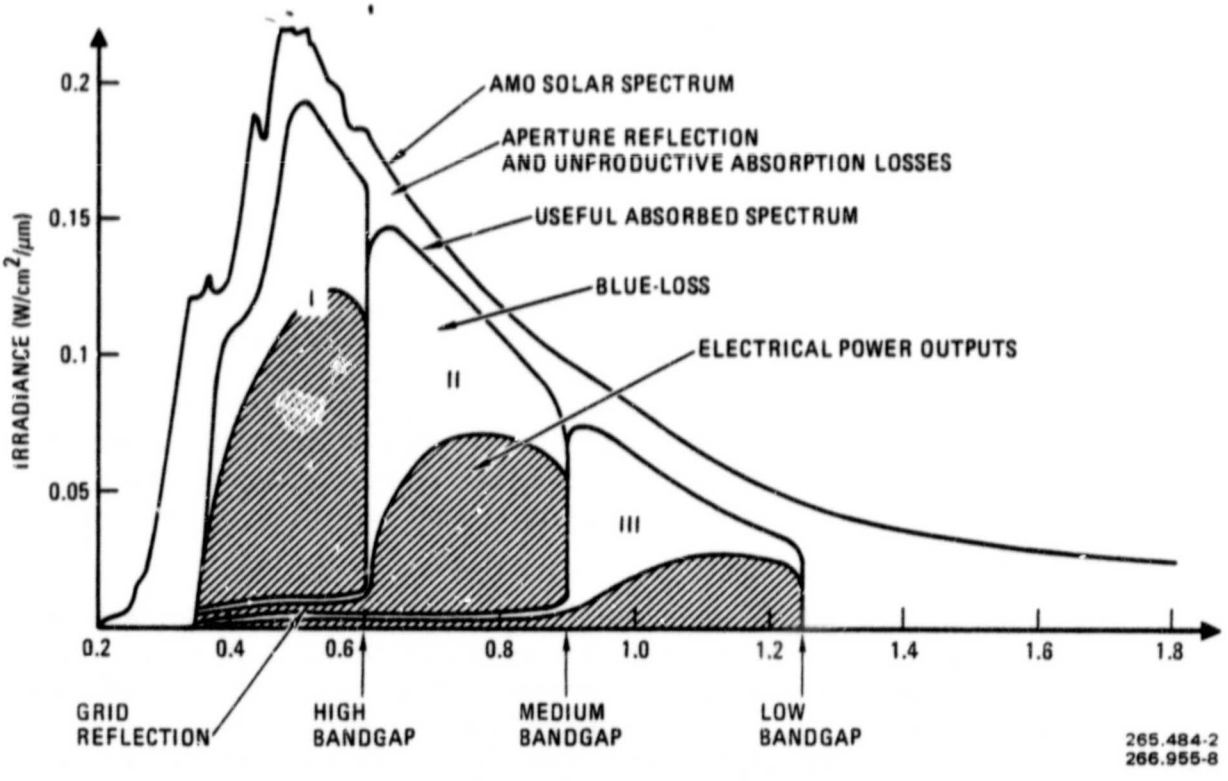

Figure 1-6. Multibandgap System Spectral Response

1.3.2 POWER COMBINING METHODOLOGY. Another feature of the reflective multibandgap configuration is the ability to combine the power output of the different bandgap materials in several ways. In one approach, power is drawn

from each cell type separately and carried on individual power busses to a centralized power management system where the power can be routed and combined to meet specific spacecraft requirements. This allows an unconstrained choice of any array of bandgaps to gain maximum photovoltaic conversion efficiency. Alternately, with an appropriate choice of bandgaps, the different cells can be combined in series or in parallel.

To combine the cells in series, the bandgaps would be chosen such that equal currents are generated in each solar cell type. The cells can then be combined without current limiting. To combine the cells in parallel, each solar cell bandgap would have to be chosen and wired in series in ratio to match voltages. For example, in the dual-bandgap configuration of Figure 1-3, two silicon cells, each generating maximum power at 0.55V, would be connected in series, and then paralleled to the AlGaAs cell operating at 1.1V. Since cell voltages are a strong function of operating temperature, the series approach is probably preferable. The predictability and consistency in current outputs of the different solar cells and the ability to parallel at the module level will allow an efficient power collection scheme to be developed. Because the main applicability of this approach will be with photovoltaic concentrators that provide improved shielding to the solar cells, environmentally induced degradations in current output will be greatly reduced. In any event, *in situ* annealing could be used to restore degraded cells such that their currents will again be closely matched.

SECTION 2
ANALYSIS OF THE REFLECTIVE MULTIBANDGAP SYSTEM

2.1 PROGRAM OBJECTIVES

The objectives of the study were:

1. To determine the maximum achievable photovoltaic conversion efficiency of this system for two, three, four, or five bandgaps, where the choice of bandgaps is unconstrained.

2. To determine the maximum achievable photovoltaic conversion efficiency of this sytem for two, three, four, and five bandgaps, where the choice of bandgaps is constrained such that:

   a. Current output is matched from each cell type.

   b. The lowest bandgap cell is silicon or germanium to allow cost reduction.

   c. The ratio of thermal load to power output is minimized.

3. To identify potential problems and limitations on the system, including a consideration of the effect of free-carrier absorption in the n-type bulk material.

4. To determine the effect of parameter changes on the optimized systems, including variations in:

   a. Quantum efficiency of the cells.

   b. Back surface reflectivity.

   c. Grid coverage.

   d. Cell thickness (which affects free-carrier absorption).

2.2 STUDY APPROACH

The study approach was divided into four tasks:

1. Review of Analysis Assumptions
2. Software Development
3. Baseline Design Analysis
4. Parametric Variations on the System

The assumptions needed to model the solar cells' configurations and responses were based on recent laboratory data, and took off from a simplified solar cell model. Software development was performed in functional block form for traceability. Additional checks of the baseline assumptions were provided by analysis of the single-bandgap case and by comparison against General Dynamics IRAD data. The analysis software was then used to find the appropriate bandgaps for achieving maximum efficiency and minimum thermal load. Variations on the system parameters were analyzed to show the elasticity of the model to changes in the assumed baseline values.

2.2.1 REVIEW OF ANALYSIS ASSUMPTIONS. The analysis performed in this work was based on a model of the response of solar cells to spectral components of the solar input flux as it passes through the reflective multibandgap system. The solar cell model is derived from the basic operation of the photovoltaic cell, and does not depend on the particular solar cell materials or electronics.

The power out of the solar cells that are being illuminated by some flux of photons of various energies can be represented by the following equation:[5]

$$\sum_{i=1}^{n} P = \left(\frac{E_g}{q}\right) (VF)_i (FF)_i \int_{\lambda=\lambda_{i-1}}^{\lambda_i} Q_i U_i(\lambda) d\lambda$$

where:

n is the number of bandgaps in the system

E_g/q is each cell's bandgap voltage

VF is each cell's voltage factor

FF is each cell's fill factor

Q is each cell's quantum efficiency

$U(\lambda)$ is the spectrum of useful absorbed light in each solar cell

λ_i is the bandgap wavelength of cell i (λ_o = 350 nm)

The number of bandgaps in the system, n, and their values, E_g, are chosen by the investigator to define the multibandgap configuration to be analyzed. The primary task of the software is to trace each spectral component of the solar flux through the system to determine which cells absorb which bands of light. This provides the values for $U(\lambda)$ for each cell as a function of wavelength. The quantum efficiency of good solar cells should be well above 90%.

This leaves the voltage factors, VF, and the fill factors, FF, as the primary source of uncertainty in the model. A review of the literature indicates that the importance of these parameters was understood early in the development of photovoltaics.

The results of an early model of voltage and fill factors at 1 sun, based on ideal solar cell parameters, are shown in Figure 2-1. The product of the VF and the FF, called the characteristic factor, CF, is also shown in the figure. In Figure 2-2, data points are plotted for laboratory demonstrations performed at a concentration of around 50 suns. As can be seen from the data, fill factors do not approach those achievable in theory, but voltage factors are improved as compared to the 1-sun case. When the product of these is taken, the characteristic factor for laboratory demonstration cells matches quite closely to the theoretical curves shown. It was therefore decided that the VF and FF be lumped together in the analysis, and the curve for the CF be used to determine the solar cell output as a function of bandgap.

Some of the other assumed parameters that determined solar cell optical performance are shown in Table 2-1. These parameters, which were also based on recent laboratory data, were variable within the analysis program. Their values were adjusted in the final portions of the analysis to show their effect on system performance. In addition to these parameters, the software made the following assumptions:

a. The Moss relation, $n_i = \sqrt[4]{173/E_g}$, was used to determine the value of the optical index of refraction as a function of bandgap.

b. UV photons with wavelengths <400 nm were assumed to be absorbed unproductively, i.e., generated waste heat.

c. Single-layer anti-reflection coatings were assumed whenever indicated in items 8 and 9 of the variables of Table 2-1.

d. Unabsorbed infrared energy beyond the lowest bandgap energy exits the system unabsorbed.

e. Free-carrier absorption was estimated[15] using the approximation $\alpha(\lambda) = 4 \times 10^{20}\, N\lambda^3$, where N is the dopant concentration and λ is wavelength in microns.

Using these parameters, an analysis of the single-bandgap case was performed as a check of the validity of the model. The variables used were as shown in Table 2-1, except that an anti-reflection coating on the cell's glass coverslide was assumed. (For the multibandgap case, the AR-coating on the glass

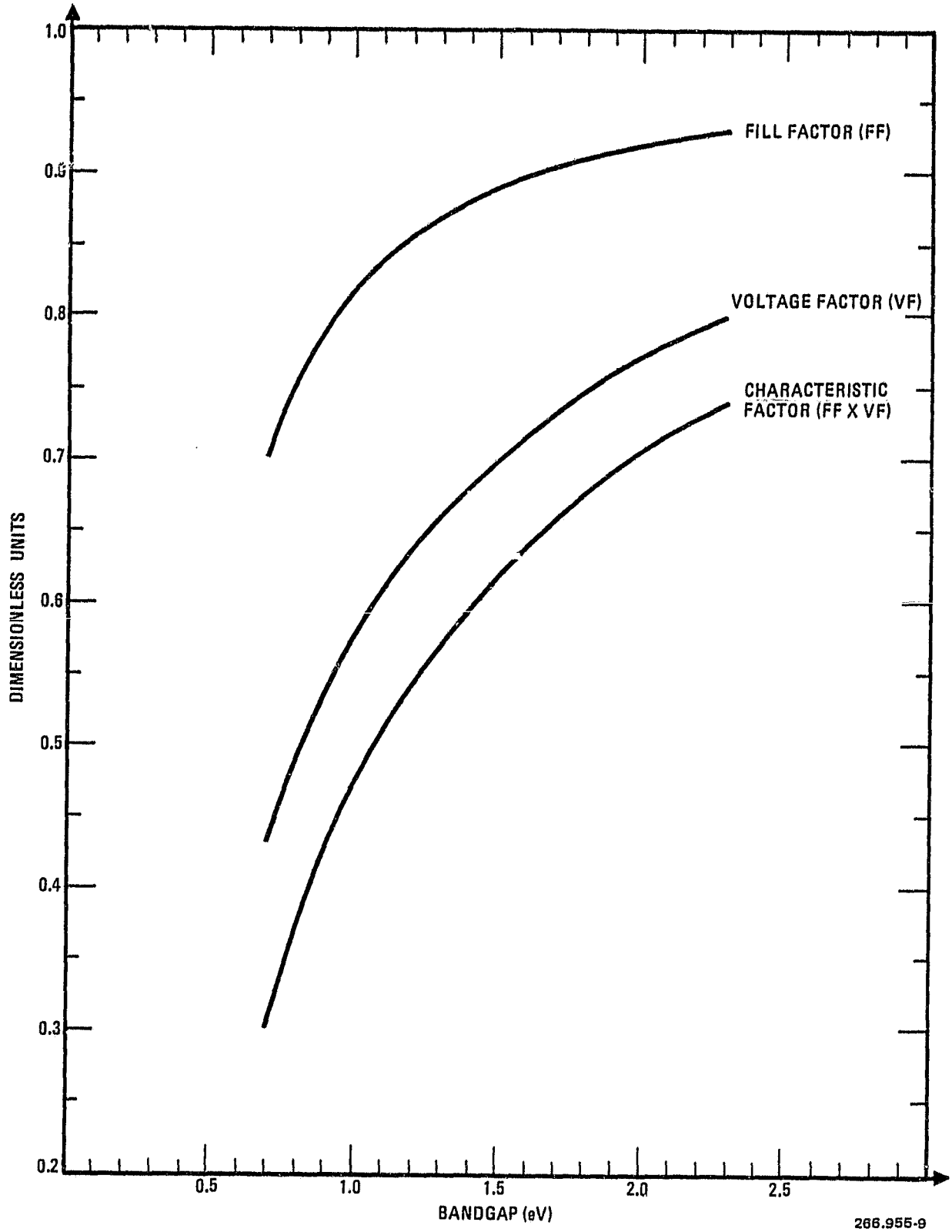

Figure 2-1. Solar Cell Performance Projections at 1 Sun, Based on Simplified Assumptions

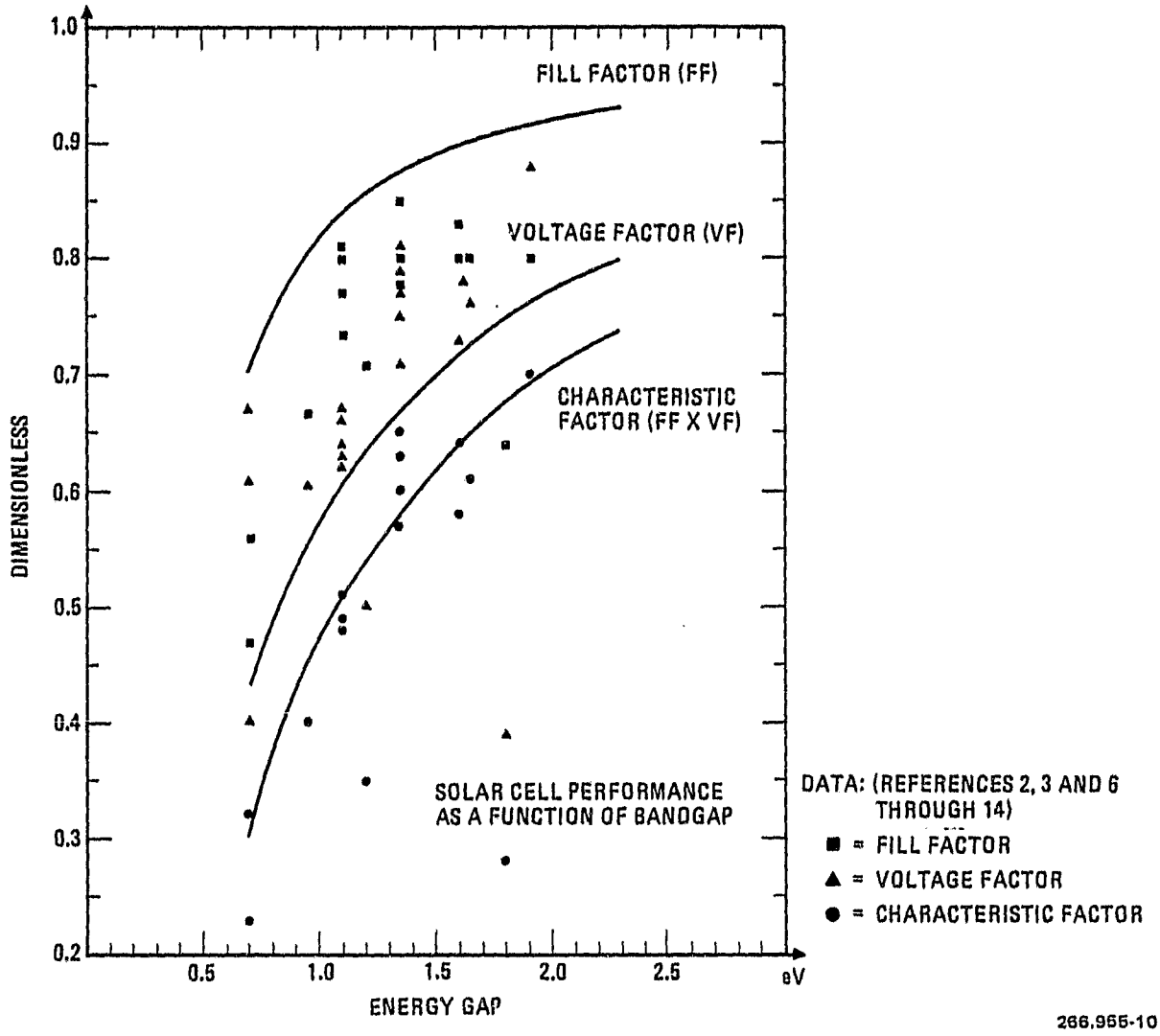

Figure 2-2. Laboratory Demonstrations at ≈ 50 Suns

was omitted because of the need to maintain total internal reflection within the glass.) The results obtained for the single-bandgap (Figure 2-3) show that the assumptions used were conservative, since silicon cells with 15% AM 0 efficiency and gallium arsenide cells with 16.5% AM 0 efficiency at 50 suns could be specified with today's technology for production items.

2.2.2 SOFTWARE DEVELOPMENT. The software was designed to perform the functions shown pictorially in Figure 2-4. Ten nanometer spectral bands from the incident solar flux are traced, one by one, through the reflective

Table 2-1. Parameters Able to be Varied Within the Program and Their Baseline Values

	Parameter	Baseline Value
1	Quantum efficiency	= 0.95
2	BSR reflectivity	= 0.95
3	Grid reflectivity	= 0.8
4	Grid coverage	= 0.1
5	Cell thickness	= 2.5E-03 cm
6	Cell size	= 0.01 cm^2
7	Concentration	= 50
8	AR-coat (cell)	= yes
9	AR-coat (glass)	= no

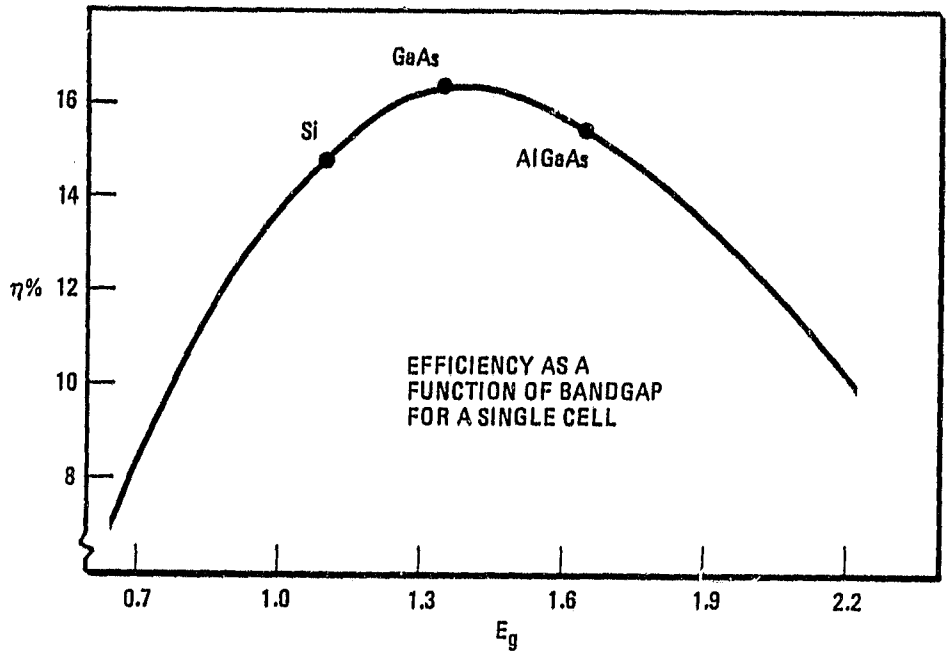

Figure 2-3. Model Results for One Bandgap

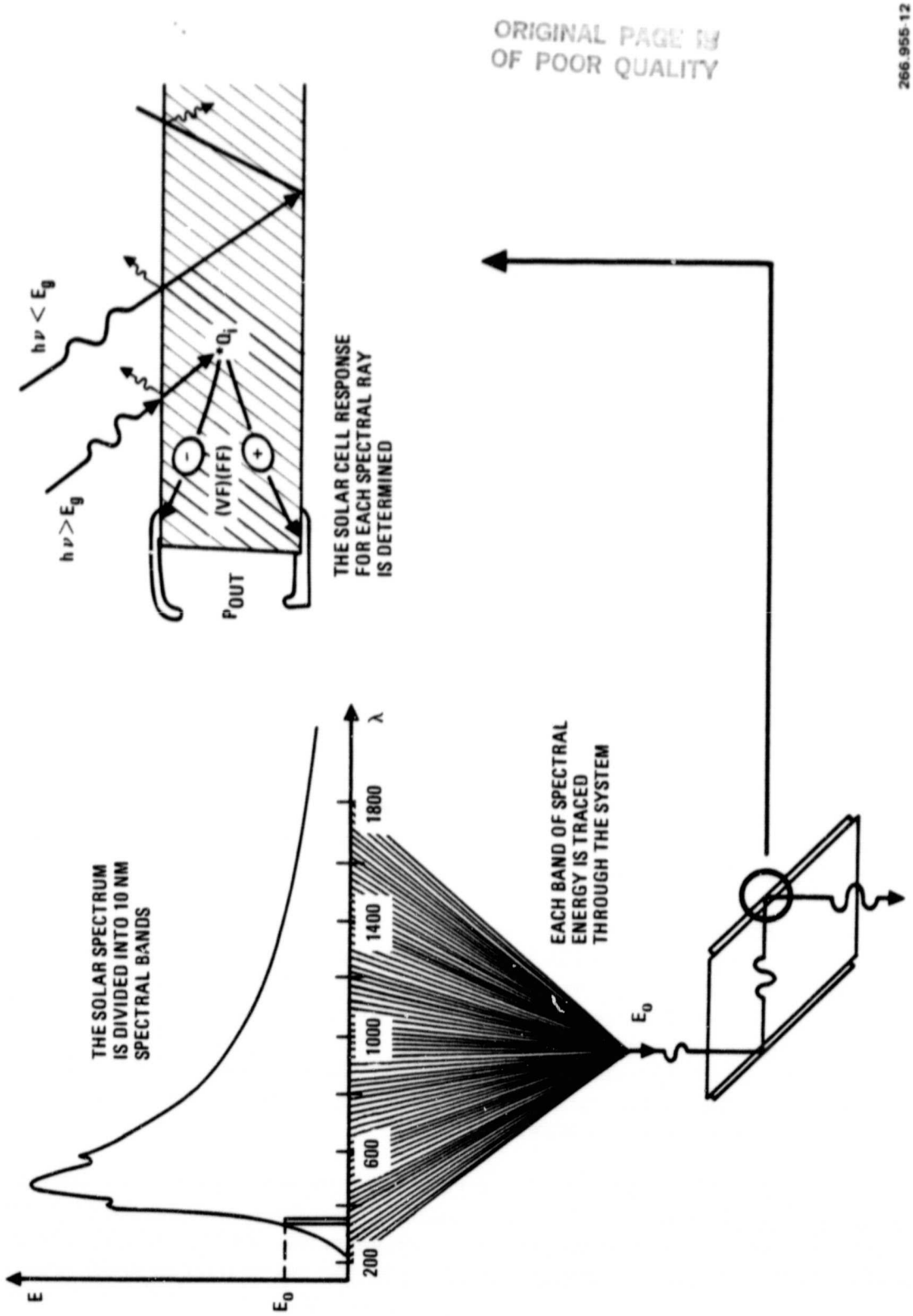

Figure 2-4. Functions Performed by the Software

multibandgap system. At each solar cell, the effect of the solar cell on the spectrum component being traced is analyzed and tracked. Certain portions of the incident beam will be reflected at the solar cell surface and by its grid lines. If the impinging beam is of an energy greater than the solar cell bandgap, the photons entering the cell are assumed to be completely absorbed within the active area, with some portion being converted to electron-hole pairs within the solar cell. For spectral components with energy less than the solar cell's bandgap, some portion is absorbed by the free carriers in the bulk and by the back surface reflector; the remainder is reflected back out of the cell and onto the next portion of the system (which may be the next solar cell or the exit aperture).

After determining, through this process, the photons in each spectral beam that are usefully absorbed by each solar cell, the software then simulates the solar cell response to this absorbed energy. This involves calculating the number of electron-hole pairs generated by each spectral component, converting these at the bandgap voltage, and multiplying by the quantum efficiency and the characteristic factor for that cell to determine the power output associated with that spectral component.

The flow charts showing the detailed procedures are in Figure 2-5. The program was divided into two modules, the first calculating the useful absorbed photons in each solar cell for each spectral beam, and the second determining the solar cells' responses to this usefully absorbed energy. Within each module, bookkeeping is performed to track those absorption processes contributing to thermal load, including grid and back surface absorption and blue loss within each spectral beam, and those losses not contributing to thermal load, such as aperture reflection and infrared rejection. A detailed program listing with definition of variables and assignment of blocks corresponding to the flow charts of Figure 2-5 is given in the appendix.

The analysis software was written so as to allow the user to vary the values of bandgaps for each of the cells in the multibandgap system. To limit the time and file space consumed by the analysis program, the ranges of bandgaps were limited to those that seemed more likely to yield reasonable results. The permissible ranges of bandgaps are shown in Table 2-2. As will be seen later, when optimized bandgap values were obtained, these values did not fall at either extreme of the bandgap ranges in all cases. This confirmed the logic in choosing these bandgap ranges.

2.2.3 ANALYSIS RESULTS. The analysis software was run for the entire range of bandgaps shown in Table 2-2 using the default parameters of Table 2-1. For the two- and three-bandgap cases, a program was written to provide a map of efficiency versus bandgap values. For the two-bandgap case, the

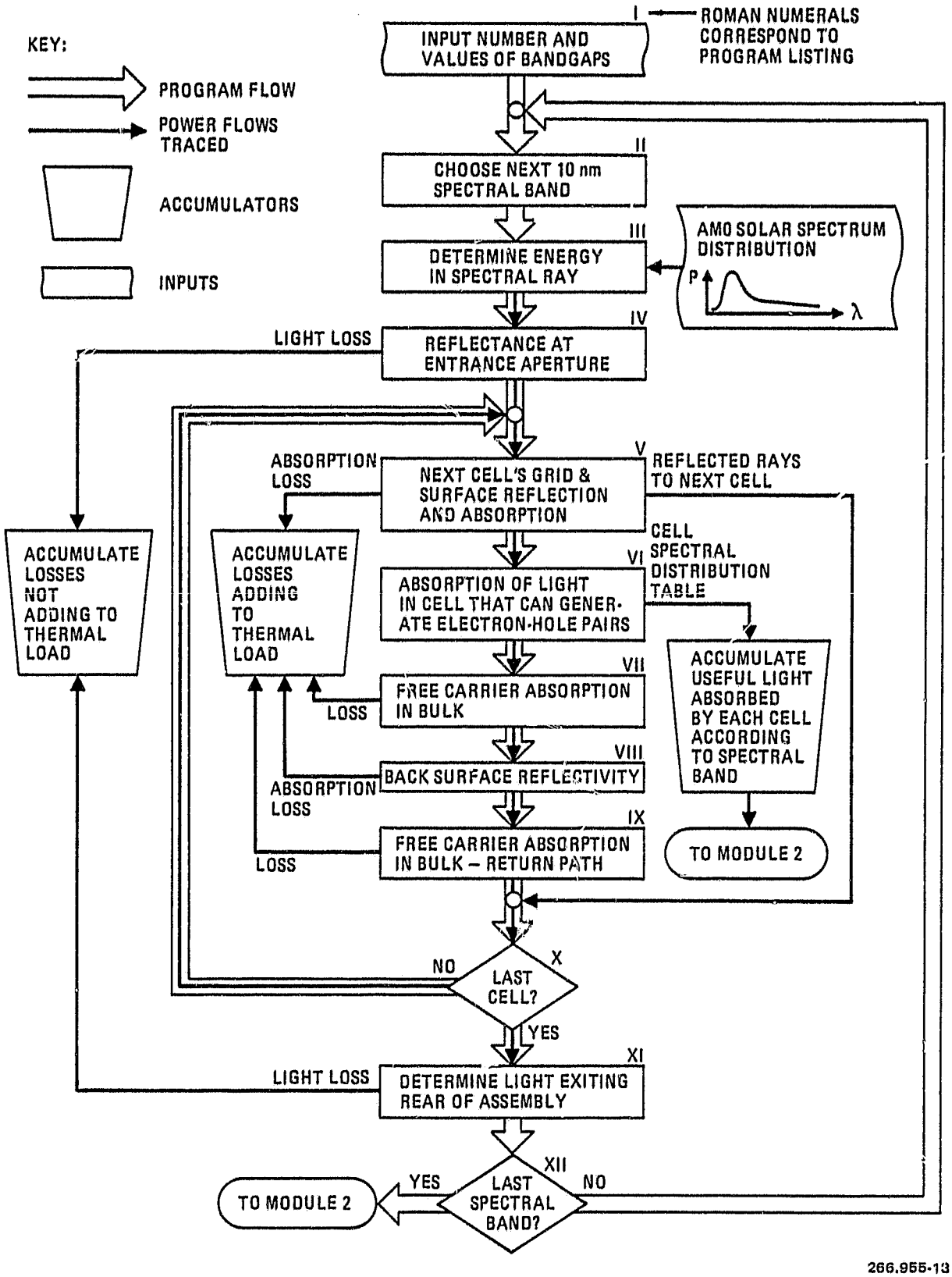

Figure 2-5a. Module 1 - Power Flows in the System

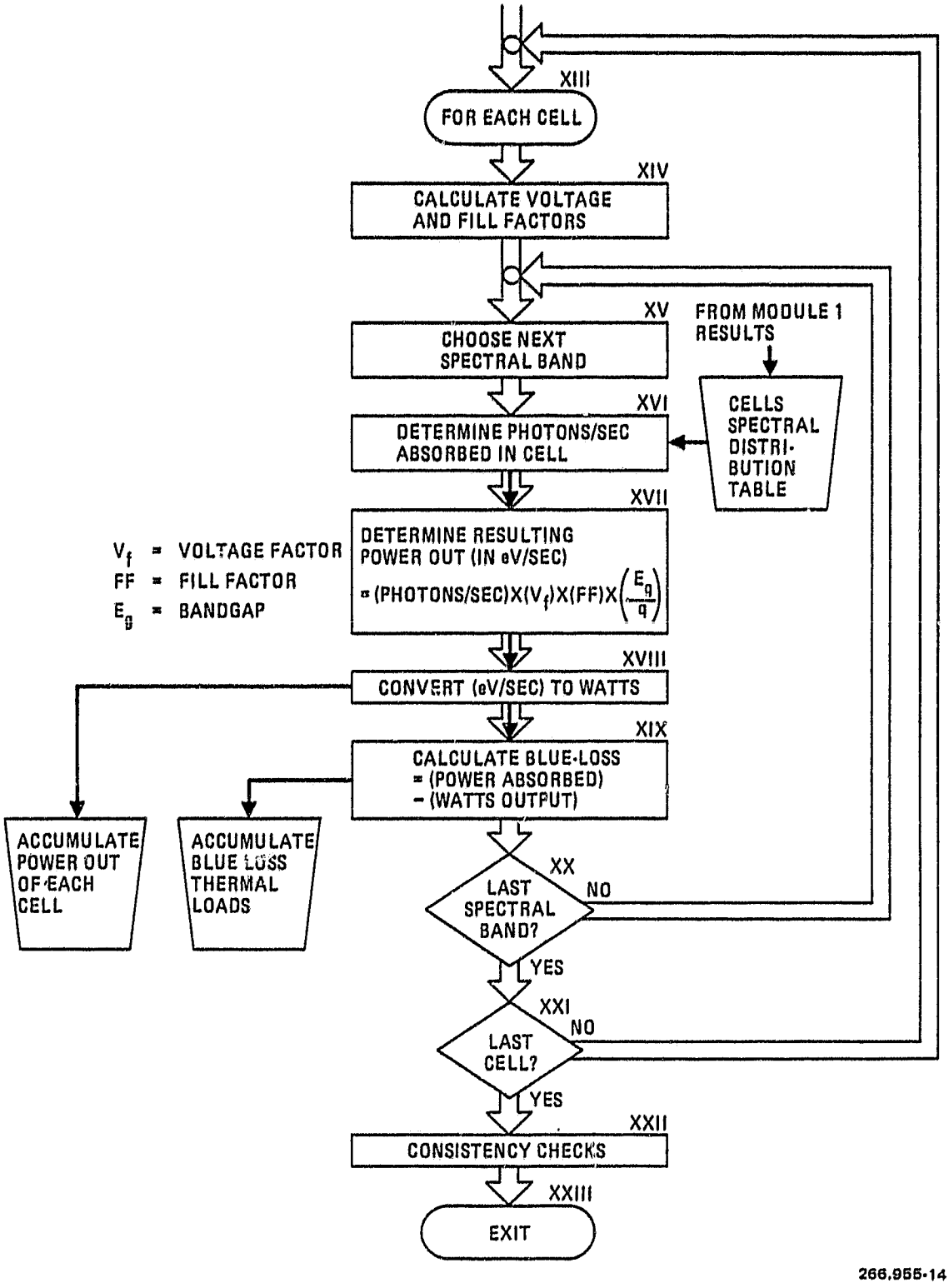

Figure 2-5b. Module 2 - Solar Cell Responses to Power Flows Determined in Module 1

Table 2-2. Range of Permissible Values Used in the Analyses

	2-Bandgap		3-Bandgap			4-Bandgap				5-Bandgap				
Value	1	2	1	2	3	1	2	3	4	1	2	3	4	5
2.2	12		7			5				4				
2.1	11		6			4				3				
2.0	10		5			3				2				
1.9	9		4			2				1	4			
1.8	8	12	3	12	12	1	5				3			
1.7	7	11	2	11	11		4				2			
1.6	6	10	1	10	10		3				1	4		
1.5	5	9		9	9		2					3		
1.4	4	8		8	8		1	5				2		
1.3	3	7		7	7			4				1	4	
1.2	2	6		6	6			3					3	
1.1	1	5		5	5			2	5				2	
1.0		4		4	4			1	4				1	4
0.9		3		3	3				3					3
0.8		2		2	2				2					2
0.7		1		1	1				1					1
Size of Output Matrix	12 × 12		7 × 12 × 12			5 × 5 × 5 × 5				4 × 4 × 4 × 4 × 4				

efficiency is plotted against the high and low bandgap values as shown in Figure 2-6. From the figure it is evident that efficiency stays high over a wide range of bandgaps, especially for the high bandgap value, which can range from 1.5 to 1.9 eV with a loss in power output of less than 3%. For the three-bandgap case, the efficiency can be plotted against high and medium bandgap values, for a given low bandgap value as shown in Figure 2-7. The figure represents one of several contour maps that could be presented for the three-bandgap case. In the map shown, the optimum efficiency point with bandgaps at 1.9, 1.3, and 0.9 eV is displayed at an efficiency of 26.5%.

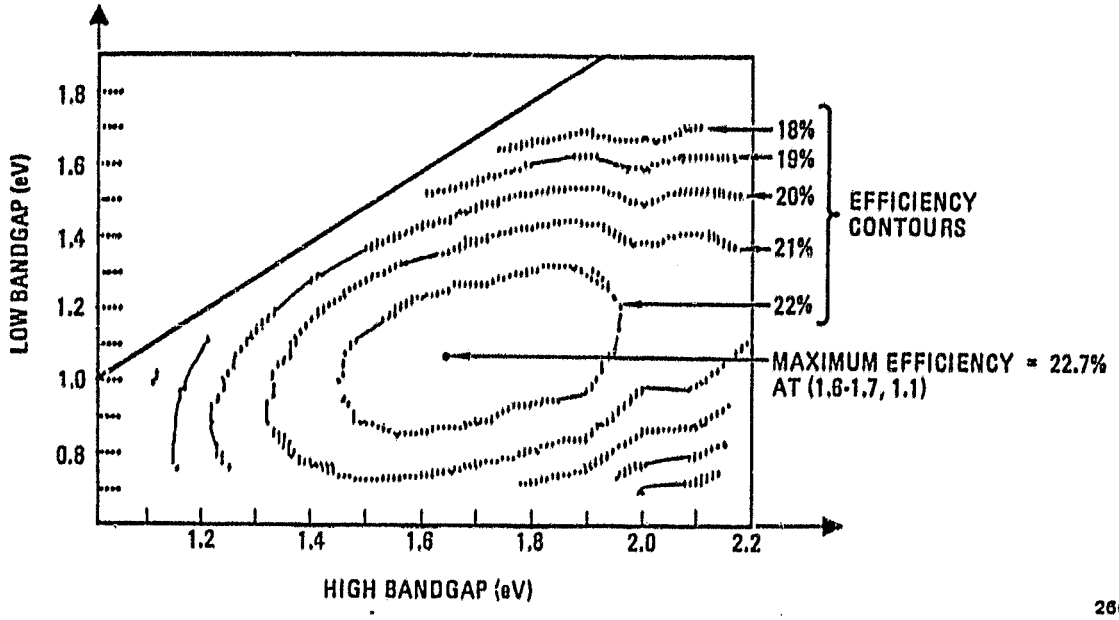

Figure 2-6. Dual-Bandgap Analysis Results

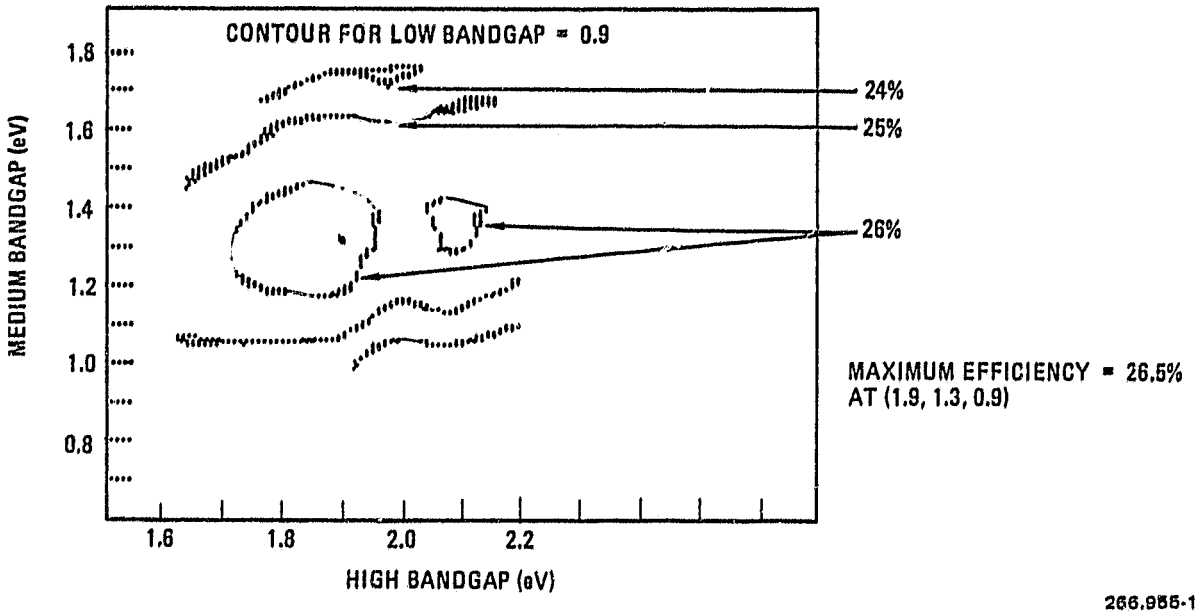

Figure 2-7. Three-Bandgap Analysis Results

It may be desirable to achieve a three-bandgap efficiency without the development of entirely new solar cell materials. For this reason, the use of an AlGaAs, GaAs, and silicon cell combination was evaluated. It was found that this combination could provide an efficiency of ∿25% under the baseline assumptions.

The optimum bandgap values, and their resultant efficiencies, are shown for the two-, three-, four-, and five-bandgap cases in Table 2-3. As one might expect, the increase in conversion efficiency diminishes as the number of bandgaps is increased. Since the additional solar cells result in increased cost to the system, a careful analysis of the fraction of total array cost attributable to solar cells should be undertaken before development of >3 bandgap systems takes place.

Table 2-3. Analysis Results Under Baseline Conditions

No. of Bandgaps	1	2	3	4	5	η (%)
2	1.7	1.1	-	-	-	22.7
3	1.9	1.3	0.9	-	-	26.5
4	2.1	1.6	1.2	0.8	-	28.6
5	2.1	1.6	1.3	1.0	0.7	29.9

As a second check of the validity of the results, the data for the two-bandgap case is shown compared against tests performed on the General Dynamics IRAD hardware. Since the IRAD hardware used a 1.65 eV AlGaAs cell illuminated with a 21-sun flux at 90C, the analysis data was corrected to account for these differences. It can be seen in Table 2-4 that the data matches quite closely with the analysis predictions.

As part of the baseline analysis, the multibandgap systems were optimized such as to minimize the ratio of thermal load to output power. The results of these runs are shown in Table 2-5. The table indicates that the thermal load is not reduced for a multibandgap system, compared to the optimized single-bandgap system, despite the increase in system efficiency.

Additional runs were performed to optimize a multibandgap system so that the currents matched. This could allow the connection of the multibandgap array into series strings to minimize complexity. The results of these runs are shown in Table 2-6. The optimized bandgaps for the current matching case are seen to closely follow those that maximize efficiency.

Table 2-4. Analysis Data Comparisons with IRAD Data

	Analysis*	IRAD
AlGaAs		
$V_{oc}xFF$	0.88	0.79 V
I_{sc}	19.7	19.8 mA/cm^2/sun
P_{out}	17.3	15.6 mW/cm^2/sun
Silicon		
$V_{oc}xFF$	0.40	0.32 V
I_{sc}	17.1	15.2 mA/cm^2/sun
P_{out}	6.8	4.9 mW/cm^2/sun
Incident energy	135.0	100.0 mW/cm^2/sun
Efficiency	17.9% (AM0) ~20.0% (AM1)	20.5% (AM1)

*Corrected for 90C IRAD temperature, 21 suns, with analysis data averaged from (1.6, 1.1) & (1.7, 1.1) to simulate IRAD bandgaps of (1.65, 1.1).

Table 2-5. Bandgaps that Minimize the Ratio of Thermal Load to Power Output (Numbers in parentheses indicate absolute thermal load as a percentage of input flux.)

Number of Bandgaps	1	2	3	4	5	Minimum Thermal Ratio	Resulting Efficiency
1	1.9	--	--	--	--	1.941 (26.2%)	13.5%
2	2.1	1.6	--	--	--	1.745 (34.0)	19.5
3	2.2	1.7	1.4	--	--	1.719 (40.2)	23.4
4	2.1	1.7	1.4	1.1	--	1.748 (47.7)	27.3
5	2.1	1.8	1.4	1.2	1	1.760 (50.5)	28.7

Table 2-6. Optimized Bandgaps for Matched Current

Number of Bandgaps	1	2	3	4	5	Resulting Efficiency	Resulting Thermal Ratio
2	1.6	1.0				22.6%	2.24
3	1.9	1.4	0.9			26.3	1.89
4	1.9	1.4	1.0	0.7		27.8	2.04
5	2.1	1.6	1.3	1.0	0.7	29.9	1.90

Finally, baseline analysis runs were performed for the case where silicon and/or germanium cells are used for the lower bandgap materials. It can be expected that these materials could provide a lower cost alternative to materials such as those of the AlGaAsSb family. The results of these runs are shown in Table 2-7. Only a slight efficiency penalty would be incurred through the use of these materials.

Table 2-7. Optimized Efficiencies using Silicon and/or Germanium

Number of Bandgaps	1	2	3	4	5	Resulting Efficiency
2	1.7-1.8	1.1				22.7%
3	2	1.4	1.1			26.0
4	1.9	1.4-1.5	1.1	0.7		27.1
5	2.1	1.6	1.3	1.1	0.7	29.9

2.2.4 PARAMETRIC VARIATIONS ON THE SYSTEM. To determine the effect of various parameters on the system performance, the assumed parameters were varied for the optimized systems found in the baseline analysis. The parameters that were examined included the back surface reflectivity, the grid area coverage, the quantum efficiency, the cell thickness as it relates to free-carrier absorption, and the concentration ratio of the impinging solar flux.

Since the reflective multibandgap solar cell concept relies on the back surface reflector as the spectrum splitting element, it is useful to know the effect of

back surface reflectivity on the system performance. Back surface reflectivities in excess of 90% have been measured on laboratory silicon cells. Their use on direct bandgap semiconductors (e.g., AlGaAs), however, has been the subject of very little examination. Since increased reflectivity of the back surface tends to increase the back contact resistance, the attainment of low series resistance may require a somewhat reduced reflectivity. Figure 2-8 shows the effect of the back surface reflectivity on the efficiency of the optimized systems of the baseline analysis. The figure shows that, for two- and three-bandgap systems, the back surface reflectivity has only a modest effect on system efficiency, and that reflectivities >70% should still result in systems with good efficiency. The rationale behind this result lies in the division of power outputs between the cells in the system. For the optimized system, about three-quarters of the output power is derived from the high bandgap cell, which is, of course, unaffected by back surface absorption losses. Additionally, the grid and surface reflections of the high bandgap cell still contribute to power output from the low bandgap cell.

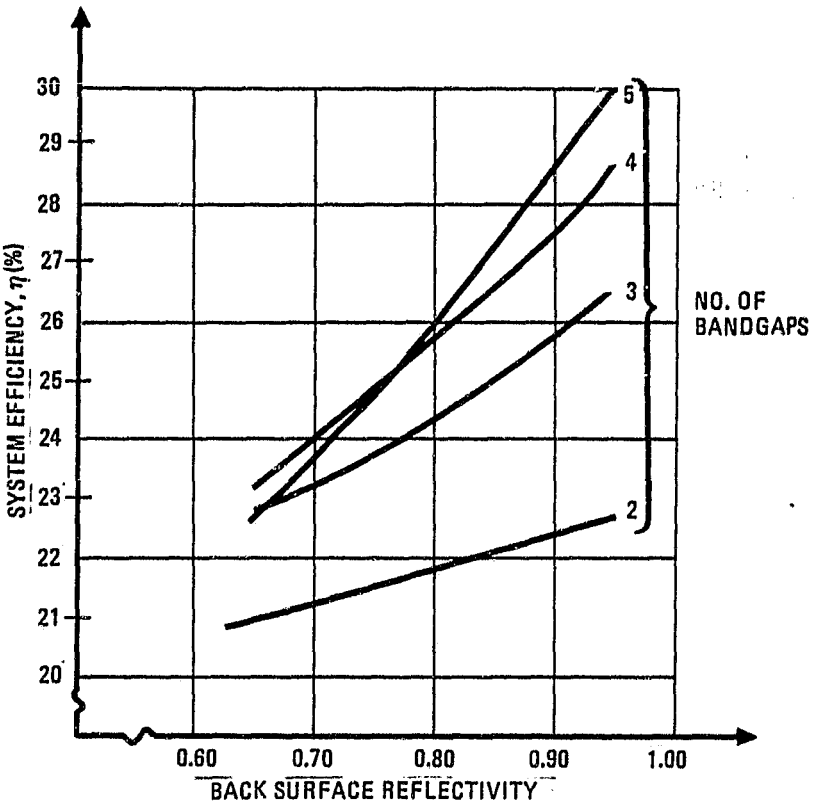

Figure 2-8. Effect of Back Surface Reflectivity on Efficiency

The effect of grid area coverage is shown in Figure 2-9. Increased grid area coverage could be used to reduce the series resistance of the solar cells. If the power loss resulting from this increased coverage is less than the additional power derived from improved series resistance, a net gain could be realized. The figure shows a linear relationship between the grid coverage and efficiency. This tends to indicate that unless the gains from reduced series resistance are dramatic, the approach of increasing the grid coverage is not desirable.

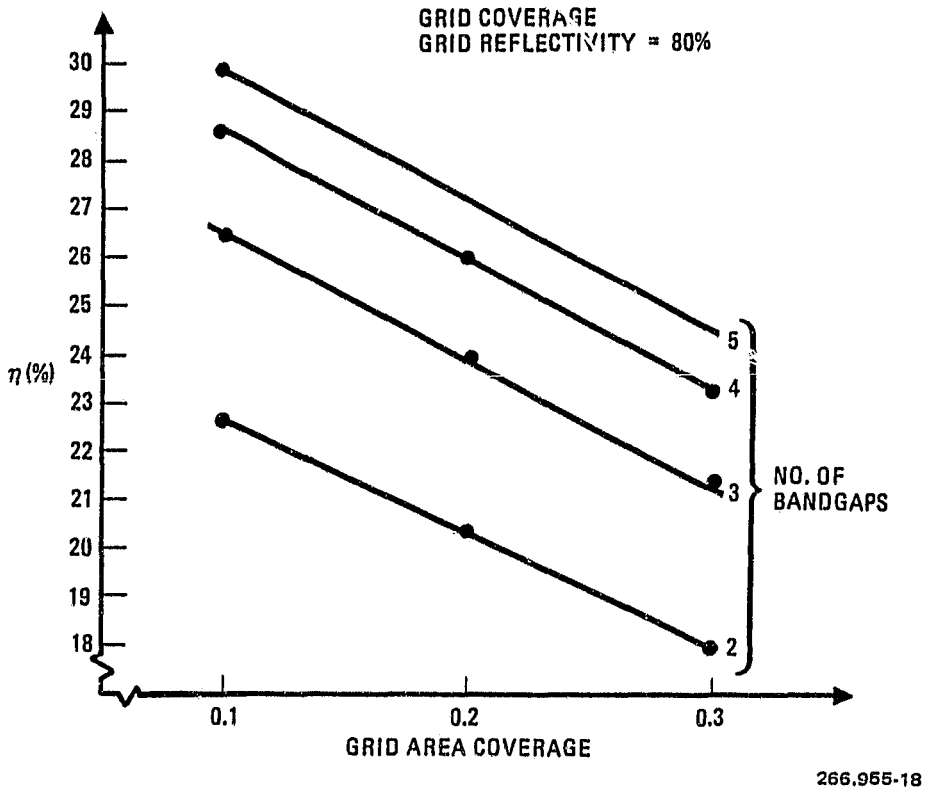

Figure 2-9. Effect of Grid Coverage on System Efficiency

The effect of quantum efficiency on the system output is shown in Figure 2-10. As might be expected, this relationship is linear, and indicates the need for achieving a high quantum efficiency if high efficiency is to be gained in the multibandgap approach.

The effect of free-carrier absorption on system performance was observed by varying the thickness of the solar cells. It was found that, even for very thick cells (>300 μm = 12 mil), free-carrier absorption was negligible according to the model. Measurements of GaAs wafers indicate a 20% absorption in the

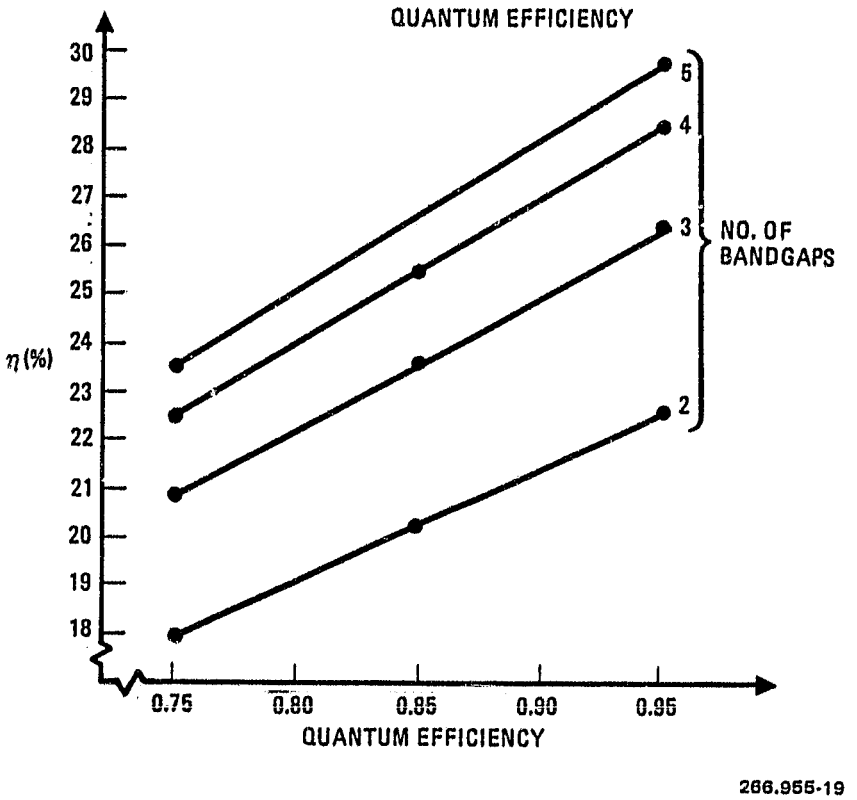

Figure 2-10. Effect of Quantum Efficiency on System Efficiency

n-type bulk at these thicknesses. It is therefore concluded that some competing absorption process besides free-carrier absorption may be responsible for bulk losses. One possibility is the absorption from valley transferred electrons in the bulk. This can occur when slightly varying energy levels arise from different crystalline orientations within the bulk. Further research is needed on absorption mechanisms within direct bandgap semiconductors.

The effect of concentration ratio on the system output efficiency is shown in Figure 2-11. Concentration voltage enhancement is accounted for in the analysis program through a perturbation applied to the characteristic factor. The short-circuit and diode currents are computed for each cell type. The effect of concentrations other than the baseline (CR = 50) is accounted by computing the new voltage factor:

$$\frac{VF_c}{VF_{50}} = \frac{\ln(C) + \ln(J_s/J_o)}{\ln(50) + \ln(J_s/J_o)}$$

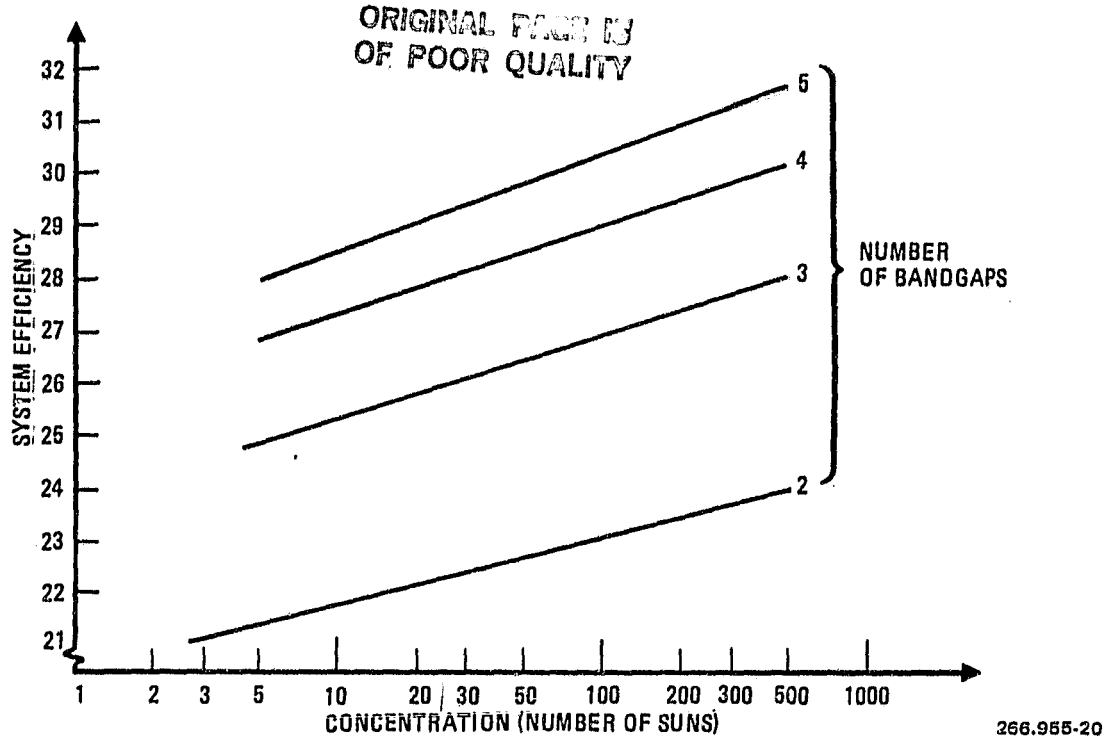

Figure 2-11. Variations of Efficiency with Concentration

The figure shows that significant gains can be achieved with higher concentrations.

2.3 CONCLUSIONS

The analysis has shown that a reflective multibandgap system can achieve efficiency improvements of >40% compared to single-bandgap systems under the same set of assumptions. Efficiencies of >22%, >26%, >28%, and >29%, for 2, 3, 4, and 5 bandgaps should be achievable with *today's* solar cell technology. The assumptions used in generating these efficiencies are conservative in that they result in a 16% efficiency when applied to a single-bandgap GaAs system alone. The bandgaps needed for optimum efficiency for the two-bandgap design (1.6-1.7, 1.1 eV) have already been under development, and General Dynamics IRAD test data has confirmed the ability to achieve >20% efficiency with this approach. For a three-bandgap system, the use of existing AlGaAs, GaAs, and silicon technology, while not of optimum bandgaps, should achieve ∿25% conversion efficiency.

The reflectivity of the back surface reflector was found to have a minor effect on the system efficiency, at least for the two- and three-bandgap cases. This

alleviates the main special requirement unique to the reflective multibandgap solar cell design. Free-carrier absorption was found to be negligible under the currently accepted model, even for thicker cells. Since laboratory data indicate a significant loss in the GaAs n-type bulk, a competing absorption process must be responsible for this effect.

2.4 RECOMMENDATIONS

The continued development of a back surface reflector AlGaAs cell of 1.65 eV bandgap would have advantages not only for implementing the reflective dual-bandgap design, but also for reducing the thermal load in a single-bandgap concentrator. Because of these benefits, the high bandgap cell development should be continued. AlGaAs cells should be able to achieve AM 0 conversion efficiencies comparable to silicon cells at comparable temperatures. Because of their higher initial voltage, and the reduced temperature in operation resulting from rejection of a greater quantity of unused beyond bandgap energy, AlGaAs cells could have higher efficiency than silicon, or even GaAs, under operating conditions.

The mechanisms for absorption within semiconductor layers and at semiconductor metal boundaries need to be understood more thoroughly. This will allow more effective implementation of solar cell optics. This includes not only the back surface reflector for this multibandgap design, but also special cell designs for reducing grid losses, and etched designs for reducing mean carrier path lengths. Only a limited amount of basic research has been done on fundamental absorption properties of III-V type materials. More is needed for a full understanding of the optical performance of these devices.

SECTION 3

REFERENCES AND BIBLIOGRAPHY

3.1 REFERENCES

1. G. W. Masden and Dr. C. E. Backus, "Increased Photovoltaic Conversion Efficiency Through Use of Spectrum Splitting and Multiple Cells," *Proceedings of the 13th IEEE Photovoltaics Specialists Conference*, Washington, D.C., June 5, 1978.

2. R. L. Moon, *et al*, "Multigap Solar Cell Requirements and the Performance of AlGaAs and Si Cells in Concentrated Sunlight," *ibid*.

3. S. W. Zehr, *et al*, "A Non-Lattice Matched Monolithic Multicolor Solar Cell," *Proceedings of the 1980 Annual Meeting of the AS of ISES*, Phoenix, Arizona, June 2, 1980.

4. T. G. Stern and L. J. Wappes, *Advanced Spacecraft Power System*, GDC-ERR-81-033, General Dynamics Convair Division, San Diego, California, December 1981.

5. S. W. Angrist, *Direct Energy Conversion*, Allyn and Bacon, Boston, Massachusetts, 1965.

6. J. Lindmayer and C. Wrigley, "Photovoltage in Concentrator Cells," *ibid (Reference 1)*.

7. Y. Z. Liu, H. T. Yang and J. S. Harris, Jr., "Low Bandgap (0.7 to 1.1 eV) Solar Cells in the GaAlAsSb/GaSb System," *Proceedings of the 14th IEEE Photovoltaics Specialists Conference*, San Diego, California, January 7, 1980.

8. M. L. Timmons and S. M. Bedair, "AlGaAsSb/GaAsSb Cascade Solar Cells," *Proceedings of the 15th IEEE Photovoltaics Specialists Conference*, Orlando, Florida, May 12, 1981.

9. E. S. Vera, J. J. Loferski and M. Spitzer, "Theoretical Limit Efficiency of Two Junction Tandem Silicon-Germanium Solar Cells Intended for Thermophotovoltaic Application," *ibid (Reference 8)*.

10. R. W. Sanderson and C. E. Backus, "The Performance of Silicon Concentrator Cells Between 50 and 500 Suns," *ibid (Reference 8)*.

11. G. W. Turner, *et al*, "GaAs Shallow-Homojunction Solar Cells," *ibid. (Reference 8).*

12. S. Khemtong, P. G. Iles, and F. Ho, "Improved Silicon Solar Cells for High Concentration Levels," *ibid (Reference 8).*

13. T. J. Maloney, "Projected Performance of III-V Epitaxial Multijunction Solar Cells in Space," *Solar Energy Materials 4:359-372,* October 1980.

14. T. J. Maloney and B. R. Cairns, "III-V Multijunction Solar Cells and III-V Solar Cells for Spectrum Splitting at Air Mass 0," *Report of Varian Associates Subcontracted Effort Contained in the Final Report, NAS3-21951,* San Diego, California, 1979.

15. J. I. Pankove, *Optical Processes in Semiconductors,* Dover Press, New York, New York, 1971.

3.2 BIBLIOGRAPHY

Bennet, A. and Olsen, L. C., "Analysis of Multiple Cell Concentrator/Photovoltaic Systems," *ibid (Reference 1),*

Spitzer, M., Lofeski, J. J. and Shewchun, J., "Theoretical Limit Efficiency of Direct Gap Solar Cells," *ibid (Reference 7).*

Pauwels, H. and DeVos, A., "Determination and Therodynamics of the Maximum Efficiency Photovoltaic Device," *ibid (Reference 8).*

Parrott, J. E. and Baird, A. M., "A Theoretical Analysis of the Optimum Number of Units in Multigap Multijunction System Under Various Operating Conditions, *ibid (Reference 8).*

LaRue, R. A., Borden, P. G. and Gregory, P. E., "A Distributed Resistance Model of an AlGaAs/GaAs Concentrator Solar Cell Illuminated with a Curved Groove Fresnel Lens," *IEEE Electron Device Letters, EDL-2:2,* February 1981.

Grosjean, C. C. and DeVos, A., "On the Upper Limit of the Energy Conversion Efficiency in Tandem Solar Cells, *J. Phys. D:Appl. Phys., 14(1981):883-94.*

APPENDIX I. RMBG PROGRAM LISTING

(Roman numerals correspond to the flow chart blocks of Figure 2-5)

```
SETUP AREA
10 D$ =  CHR$ (4)
15  DIM S1%(4,4,4,4,4,4),EFF(5),TR%(4,4,4,4,4,4)
20  DIM P2OUT(5),THC(5),POUT(5),VF(5),FF(5),BLUE(5),BGAP(5),CUTWAV(5),SDIST(5
    ,250),CREF(5),CTHERM(5),H10(6),L10(5)
30 QEFF = 0.95:BSREF = 0.95:RGIRID = 0.8:GAREA = 0.1:CTHICK = 0.0025:CSIZE =
    0.01:NSUNS = 50:GLINDEX = 1.5:NDOP = 1E18:COEF = 4E - 20:CAR$ = "YES":GA
    R$ = "NO"
35 B3 = 3:B4 = 2:B5 = 1: REM  DUMMY VALUES USED IN LATER TESTS WHEN NGAP<5
36 HH(1) = 2.2:LL(1) = 1.9:HH(2) = 1.9:LL(2) = 1.6:HH(3) = 1.6:LL(3) = 1.3:HH
    (4) = 1.3:LL(4) = 1:HH(5) = 1:LL(5) = 0.7
37 T0 = 10:E6 =  - 2E - 6: REM  CONSTANTS
40  PRINT "THE FOLLOWING ARE THE DEFAULT PARAMETERS
50  PRINT "(1)QUANTUM EFF    = ";QEFF: PRINT "(2)BSR REFLECT'Y = ";BSREF: PRINT
    "(3)GRID REFLECT'Y= ";RGIRID: PRINT "(4)GRID COVERAGE = ";GAREA: PRINT "
    (5)CELL THICKNESS= ";CTHICK;"CM"
60  PRINT "(6)CELL SIZE      = ";CSIZE;"CMX*2": PRINT "(7)CONCENTRATION = ";NS
    UNS
65  PRINT "(8)AR-COAT (CELL)= ";CAR$: PRINT "(9)AR-COAT(GLASS)= ";GAR$: PRINT
    : INPUT "TO CHANGE A PARAMETER, INPUT ITS NUMBER - OTHERWISE ENTER A ZER
    0 - ?";CHANGE
70  IF CHANGE = 0 THEN 90
71  IF CHANGE = 1 THEN 81
72  IF CHANGE = 2 THEN 82
73  IF CHANGE = 3 THEN 83
74  IF CHANGE = 4 THEN 84
75  IF CHANGE = 5 THEN 85
76  IF CHANGE = 6 THEN 86
77  IF CHANGE = 7 THEN 87
78  IF CHANGE = 8 THEN 88
79  IF CHANGE = 9 THEN 89
80  GOTO 1030
81  INPUT "ENTER NEW QUANTUM EFFICIENCY";QEFF: GOTO 50
82  INPUT "ENTER NEW BACK SURFACE FEFLECTIVITY";BSREF: GOTO 50
83  INPUT "ENTER NEW GRID REFLECTIVITY";RGIRID: GOTO 50
84  INPUT "ENTER NEW GRID AREA COVERAGE";GAREA
85  INPUT "ENTER NEW CELL THICKNESS";CTHICK: GOTO 50
86  INPUT "ENTER NEW CELL SIZE";CSIZE: GOTO 50
87  INPUT "ENTER NEW CONCENTRATION";NSUNS: GOTO 50
88  INPUT "ENTER AR-COATING FOR CELL (YES OR NO)";CAR$: GOTO 50
89  INPUT "ENTER AR-COATING FOR GLASS(YES OR NO)";GAR$: GOTO 50
90  PRINT D$;"OPEN SOLAR SPECTRUM"
91  PRINT D$;"READ SOLAR SPECTRUM"
92  FOR I = 1 TO 250: INPUT SDIST(0,I): NEXT I: REM  DATA PUT HERE TO SAVE RO
    OM
93  PRINT D$;"CLOSE SOLAR SPECTRUM"
94  INPUT "NUMBER OF BANDGAPS - ";NGAP: PRINT : PRINT "EACH BANDGAP RANGE MUS
    T BE INPUT IN     MULTIPLES OF 0.1 EV": PRINT
95  PRINT : FOR I = 1 TO NGAP: PRINT : PRINT "BANDGAP#";I: PRINT "PICK HIGH A
    ND LOW VALUES": PRINT "BETWEEN ";HH(I);" AND ";LL(I): INPUT "ENTER HIGH
    VALUE";HGAP: INPUT "ENTER LOW  VALUE";LGAP
I
96 H10(I) = HGAP * 10:L10(I) = LGAP * 10: NEXT I
97  FOR B1 = H10(1) TO L10(1) STEP  - 1: FOR B2 = H10(2) TO L10(2) STEP  - 1:
    FOR B3 = H10(3) TO L10(3) STEP  - 1: FOR B4 = H10(4) TO L10(4) STEP  -
    1: FOR B5 = H10(5) TO L10(5) STEP  - 1
98 BGAP(1) = B1 / 10:BGAP(2) = B2 / 10:BGAP(3) = B3 / 10:BGAP(4) = B4 / 10:BG
    AP(5) = B5 / 10
100  IF BGAP(1) <  = BGAP(2) OR BGAP(2) <  = BGAP(3) OR BGAP(3) <  = BGAP(4) OR
    BGAP(4) <  = BGAP(5) THEN 720
```

```
I
  101  FOR I = 1 TO NGAP
  102  PRINT BGAP(I);CINDEX =  SQR ( SQR (173 / BGAP(I)));CREF(I) = (CINDEX - G
       LIND) * (CINDEX - GLIND) / (CINDEX + GLIND) / (CINDEX + GLIND);CUTWAV(I)
        = 1240 / BGAP(I)
  103  IF CAR$ = "YES" THEN CREF(I) = CREF(I) / 2
  104  NEXT I: PRINT : PRINT
  105 REFG = (GLIND - 1) * (GLIND - 1) / (GLIND + 1) / (GLIND + 1);FCAR = NDOP *
       COEF
  106  IF CAR$ = "YES" THEN REFG = REFG / 2
II    110  FOR I = 1 TO 250
III   115 RAY = SDIST(0,I)
IV
  120 APREF = APREF + REFG * RAY
  130 RAY = RAY * (1 - REFG)
  140  IF I < 40 THEN GTHERM = GTHERM + RAY: GOTO 230
V
  145  FOR N = 1 TO NGAP
  150 RREF = GAREA * RGIRID * RAY + CREF(N) * RAY
  160 CTHERM(N) = CTHERM(N) + (1 - RGIRID) * GAREA * RAY
  170 RAY = RAY - RREF - (1 - RGIRID) * GAREA * RAY
VI    180  IF CUTWAV(N) / 10 > I + 1 THEN CAB = RAY;SDIST(N,I) = SDIST(N,I) + CAB;R
       AY = RREF: GOTO 205
VII
VIII
  190  IF  INT (CUTWAV(N) / T0) = I THEN CAB = (CUTWAV(N) / T0 - I) / T0 * RAY;
       SDIST(N,I) = CAB;DT = (RAY - CAB) * (1 -  EXP (FCAR * E6 * I * I * I * C
       THICK) * BSREF);CTHERM(N) = CTHERM(N) + DT;RAY = RAY + RREF - CAB - DT: GOT
       205
IX
X
  200  IF CUTWAV(N) / T0 < I THEN DT = RAY * (1 -  EXP (FCAR * E6 * I * I * I *
       CTHICK) * BSREF);CTHERM(N) = CTHERM(N) + DT;RAY = RAY + RREF - DT
  205  NEXT N
XI
  210 EXIT = EXIT + RAY
  220 NTHLOSS = EXIT + APREF
XII   230  NEXT I
      490 K1 = 2.1186:K2 =  - 0.6528:K3 =  - 1.015
XIII  500  FOR N = 1 TO NGAP
XIV   510 CF(N) = K1 *  SQR (BGAP(N)) + K2 * BGAP(N) + K3
      515 JS = 0
XV    520  FOR I = 1 TO 250
XVI   530 PHPSEC = SDIST(N,I) * I / 124
      535 JS = JS + PHPSEC * QEFF
XVII  540 EVPSEC = PHPSEC * QEFF * CF(N) * BGAP(N)
XVIII 550 POUT(N) = POUT(N) + EVPSEC
XIX   560 BLUE(N) = BLUE(N) + SDIST(N,I) - EVPSEC
XX    570  NEXT I
ADJUSTMENT FOR CONCENTRATION
  575  IF NSUNS = 50 THEN 580
  576 J0 = 1E9 /  EXP (BGAP(N) / .026)
  577 K4 = ( LOG (NSUNS) +  LOG (JS / J0)) / ( LOG (50) +  LOG (JS / J0))
  579 POUT(N) = POUT(N) * K4:BLUE(N) = BLUE(N) - POUT(N) + POUT(N) / K4
XXI   580  NEXT N
XXII
  585 S2 = 0:S3 = 0
  586 I1 = BGAP(1) * 10 - 16:I2 = BGAP(2) * 10 - 15:I3 = BGAP(3) * 10 - 12:I4 =
       BGAP(4) * 10 - 9:I5 = BGAP(5) * 10 - 6
  590  FOR N = 1 TO NGAP:EFF(N) =  INT (POUT(N) / .135):THC(N) =  INT (100 * (B
       LUE(N) + CTHERM(N))) / 100:P2OUT(N) =  INT (POUT(N) * 100) / 100:S1%(I1,
       I2,I3,I4,I5) = S1%(I1,I2,I3,I4,I5) + EFF(N):S2 = S2 + THC(N):S3 = S3 + P
       2OUT(N): NEXT N
  620  PRINT "CELL #  BGAP  EFF'Y  POUT  THERM"
  630  PRINT "------  -----  -----  ----  -----"
  640  FOR N = 1 TO NGAP: PRINT "  ";N;"     ";BGAP(N);"  ";EFF(N);"  ";P2OUT(N);
       "  ";THC(N): NEXT N
  645  PRINT "------------  -----  ----  -----": PRINT "SYSTEM TOTAL";S1%(I1,I2,I3
       ,I4,I5);"  ";S3;"  ";S2
  646  PRINT : PRINT
  650  PRINT "APERTURE REFLECTION = ";APREF
  660  PRINT "INFRA-RED REJECTION = ";EXIT
  670  PRINT "GLASS THERMAL LOAD  = ";GTHERM
  680  FOR N = 1 TO NGAP:TSUM = TSUM + BLUE(N) + CTHERM(N):PSUM = PSUM + POUT(N
       ): NEXT N
  690 TSUM = TSUM + GTHERM
  700  PRINT "TOTAL THERMAL LOAD = ";TSUM
  705 TR%(I1,I2,I3,I4,I5) = TSUM / PSUM * 100
```

```
      706  PRINT "THERMAL/POWER RATIO=";TR%(I1,I2,I3,I4,I5)
      710  PRINT "CONSISTENCY TOTALS = ";TSUM + PSUM + NTHLOSS
      715 APREF = 0:GTHERM = 0:EXIT = 0:PSUM = 0:TSUM = 0: FOR J = 1 TO 5:CTHERM(J)
          = 0:POUT(J) = 0:BLU(J) = 0: FOR K = 1 TO 250:SDIST(J,K) = 0: NEXT K: NEXT
          J
XXII  716  PRINT : PRINT
      720  NEXT B5
      730  NEXT B4
      740  NEXT B3
      750  NEXT B2
      760  NEXT B1
      765  INPUT "OK TO STORE NEW FILES?";DUMMY$: IF DUMMY$ < > "YES" THEN 1030
      770  PRINT D$;"OPEN EFFILE 5"
      780  PRINT D$;"DELETE EFFILE 5"
      790  PRINT D$;"OPEN EFFILE 5"
      800  PRINT D$;"WRITE EFFILE 5"
      900  FOR I = 1 TO 4: FOR J = 1 TO 4: FOR K = 1 TO 4: FOR L = 1 TO 4: FOR M =
          1 TO 4: PRINT S1%(I,J,K,L,M): NEXT M: NEXT L: NEXT K: NEXT J: NEXT I
      910  PRINT D$;"CLOSE EFFILE 5"
XXIII 970  PRINT D$;"OPEN TRFILE 5"
      980  PRINT D$;"DELETE TRFILE 5"
      990  PRINT D$;"OPEN TRFILE 5"
     1000  PRINT D$;"WRITE TRFILE 5"
     1010  FOR I = 1 TO 4: FOR J = 1 TO 4: FOR K = 1 TO 4: FOR L = 1 TO 4: FOR M =
          1 TO 4: PRINT TR%(I,J,K,L,M): NEXT M: NEXT L: NEXT K: NEXT J: NEXT I
     1020  PRINT D$;"CLOSE TRFILE 5"
     1030  STOP
```

"RMBG ANALYSIS" PROGRAM - DEFINITION OF VARIABLES

The following list describes variables used in the analysis program in order of their appearance:

D$ = Disk control character for the Apple II computer

S1(i,j,...,n) = N-dimensional array used to store the efficiency results for all combinations of N-bandgaps (see Table 2-2 for definition of index values)

EFF(i) = efficiency of the i-th cell in the bandgap combination being considered (highest bandgap is #1, etc.)

TR(i,j,...,n) = N-dimensional array used to store the thermal/power ratio results for all combinations of N-bandgaps

SPECTRUM(i) = i-th element contains the energy in the solar spectrum (mW/cm**2) from (10*i)nm to (10*(i+1))nm

THC(i) = thermal load of the i-th cell in the bandgap combination being considered (mW)

POUT(i) = power output of the i-th cell (mW)

BLUE(i) = blue loss of the i-th cell (mW)

BGAP(i) = bandgap of the i-th cell (eV)

CUTWAV(i) = cutoff wavelength corresponding to the bandgap of the i-th cell (nm)

SDIST(i,m) = useful power absorbed by the i-th cell from the m-th spectral band (mW)

CREF(i) = reflectivity of the i-th cell

CTHERM(i) = total thermal load on i-th cell (mW)

H1O(i),L1O(i) = ten times the high and low value for the range of values for the i-th cell

QEFF = quantum efficiency for all cells

BSREF = back surface reflectivity for all cells

RGIRID = reflectivity of the current collection grid for all cells

GAREA = fraction of cell surface covered by the current collection grid

CTHICK = thickness of all cells (cm)

CSIZE = size of all cells (cm**2)

NSUNS = number of suns of concentration at the system entrance aperture

GLINDEX = index of refraction of all glass in the system

NDOP = n-type doping of all cells (1/cm**3)

COEF = coefficient in the equation for free carrier absorption

CHANGE = flag indicating a user desired change of parameters

NGAP = number of bandgaps for the analysis

HGAP,LGAP = high and low of the bandgaps to analyze, as input by the user

CINDEX = index of refraction computed for each cell

B1,B2,...,Bn = looping variables for each range of n bandgaps

REFG = glass aperture reflectivity

FCAR = factor which, when multiplied by cell thickness, gives the extinction coefficient for each cell from free-carrier absorption

RAY = energy in the spectral ray being traced

APREF = energy reflected at the glass aperture (mW)

EXIT = infra-red energy exiting the system

NTHLOSS = losses not contributing to system thermal load

K1,K2,K3 = best fit coefficients for equation describing the characteristic factor as a function of bandgap

CF(i) = characteristic factor of i-th cell

PHPSEC = number of useful photons absorbed in each cell

EVPSEC = energy output of each cell in eV/sec

JS = solar cell light generated current

JO = solar cell diode current

K4 = factor used to adjust solar cell output at different concentrations

I1,I2,I3 = index used to store results in S1(i,j,...,n) and TR(i,j,...,n) - see Table 2-2

TSUM = total thermal load on the system